Improved limit on the muon electric dipole moment

G. W. Bennett,[2] B. Bousquet,[10] H. N. Brown,[2] G. Bunce,[2] R. M. Carey,[1] P. Cushman,[10] G. T. Danby,[2] P. T. Debevec,[8] M. Deile,[13] H. Deng,[13] W. Deninger,[8] S. K. Dhawan,[13] V. P. Druzhinin,[3] L. Duong,[10] E. Efstathiadis,[1] F. J. M. Farley,[13] G. V. Fedotovich,[3] S. Giron,[10] F. E. Gray,[8] D. Grigoriev,[3] M. Grosse-Perdekamp,[13] A. Grossmann,[7] M. F. Hare,[1] D. W. Hertzog,[8] X. Huang,[1] V. W. Hughes,[13,*] M. Iwasaki,[12] K. Jungmann,[6] D. Kawall,[13] M. Kawamura,[12] B. I. Khazin,[3] J. Kindem,[10] F. Krienen,[1,*] I. Kronkvist,[10] A. Lam,[1] R. Larsen,[2] Y. Y. Lee,[2] I. Logashenko,[1,3] R. McNabb,[10,8] W. Meng,[2] J. Mi,[2] J. P. Miller,[1] Y. Mizumachi,[11] W. M. Morse,[2] D. Nikas,[2] C. J. G. Onderwater,[8,6] Y. Orlov,[4] C. S. Özben,[2,8] J. M. Paley,[1] Q. Peng,[1] C. C. Polly,[8] J. Pretz,[13] R. Prigl,[2] G. zu Putlitz,[7] T. Qian,[10] S. I. Redin,[3,13] O. Rind,[1] B. L. Roberts,[1] N. Ryskulov,[3] S. Sedykh,[8] Y. K. Semertzidis,[2] P. Shagin,[10] Yu. M. Shatunov,[3] E. P. Sichtermann,[13] E. Solodov,[3] M. Sossong,[8] A. Steinmetz,[13] L. R. Sulak,[1] C. Timmermans,[10] A. Trofimov,[1] D. Urner,[8] P. von Walter,[7] D. Warburton,[2] D. Winn,[5] A. Yamamoto,[9] and D. Zimmerman[10]

(Muon ($g-2$) Collaboration)

[1]*Department of Physics, Boston University, Boston, Massachusetts 02215, USA*
[2]*Brookhaven National Laboratory, Upton, New York 11973, USA*
[3]*Budker Institute of Nuclear Physics, 630090 Novosibirsk, Russia*
[4]*LEPP, Cornell University, Ithaca, New York 14853, USA*
[5]*Fairfield University, Fairfield, Connecticut 06430, USA*
[6]*Kernfysisch Versneller Instituut, University of Groningen, NL-9747 AA, Groningen, The Netherlands*
[7]*Physikalisches Institut der Universität Heidelberg, 69120 Heidelberg, Germany*
[8]*Department of Physics, University of Illinois at Urbana-Champaign, Urbana, Illinois 61801, USA*
[9]*KEK, High Energy Accelerator Research Organization, Tsukuba, Ibaraki 305-0801, Japan*
[10]*Department of Physics, University of Minnesota, Minneapolis, Minnesota 55455, USA*
[11]*Science University of Tokyo, Tokyo, 153-8902, Japan*
[12]*Tokyo Institute of Technology, 2-12-1 Ookayama, Meguro-ku, Tokyo, 152-8551, Japan*
[13]*Department of Physics, Yale University, New Haven, Connecticut 06520, USA*
(Received 11 November 2008; published 21 September 2009)

Three independent searches for an electric dipole moment (EDM) of the positive and negative muons have been performed, using spin precession data from the muon $g-2$ storage ring at Brookhaven National Laboratory. Details on the experimental apparatus and the three analyses are presented. Since the individual results on the positive and negative muons, as well as the combined result, $d_\mu = (0.0 \pm 0.9) \times 10^{-19} e$ cm, are all consistent with zero, we set a new muon EDM limit, $|d_\mu| < 1.8 \times 10^{-19} e$ cm (95% C.L.). This represents a factor of 5 improvement over the previous best limit on the muon EDM.

DOI: 10.1103/PhysRevD.80.052008 PACS numbers: 13.40.Em, 12.15.Lk, 14.60.Ef

I. INTRODUCTION

A permanent electric dipole moment (EDM) for a particle in a nondegenerate state violates both parity (P) and time reversal (T) symmetries. Assuming conservation of the combined symmetries CPT, where C refers to charge conjugation symmetry, T violation implies CP violation. Unlike parity violation, which is maximal in weak leptonic decays, CP violation has never been observed in the leptonic sector. Given the small observed levels of CP violation (seen only in the decays of neutral kaons and B mesons), the standard model (SM) predicts that the EDMs of the leptons are so small that their detection is well beyond experimental capabilities for the foreseeable future. Any nonzero experimental value would therefore indicate the existence of new physics. This distinguishes leptons from strongly interacting particles, which could have a measurable SM EDM if the $\bar{\theta}$ parameter in the QCD Lagrangian turned out to be sufficiently large. Most models purporting to explain the baryon asymmetry of the Universe require CP violation [1], but the observed level in the B-meson and kaon systems is insufficient, suggesting that there must be other, as yet undetected sources of CP violation, which could produce nonvanishing EDMs. Consequently, experimental searches for EDMs are being widely pursued. The muon is of special interest because, again for the foreseeable future, it is the only particle, outside the first generation, for which a precision EDM measurement is feasible [2].

The best experimental limits on the EDMs of elementary particles or atoms, some of which are listed in Table I, are those for the ^{199}Hg atom, the electron, and the neutron. The

*Deceased.

TABLE I. Some experimental limits on EDMs.

Physical system	Limit (e cm), C.L.	Reference
^{199}Hg atom	3.1×10^{-29}, 95%	[3]
Electron	1.6×10^{-27}, 90%	[4]
Neutron	2.9×10^{-26}, 90%	[5]
Muon	1.05×10^{-18}, 95%	[6]

measured values are all consistent with zero. These stringent limits, which are likely to improve over the next few years, have produced some of the most significant constraints on extensions to the SM, many of which predict relatively large EDMs [7–10]. The data on the neutron lead to the current limit [11], $\bar{\theta} < 10^{-10}$.

The current limit on the muon EDM [6], set by the last muon $g-2$ experiment at CERN and also shown in Table I, is considerably less stringent. In the SM and in some of its extensions, the lepton EDMs scale with mass. Scaling the measured electron EDM by the ratio of the muon to the electron mass implies a limit for the muon of $d_\mu = (1.4 \pm 1.5) \times 10^{-25} e$ cm. However, the scaling which could come from new physics is essentially unknown. Indeed, some SM extensions predict that the muon EDM is larger than $10^{-23} e$ cm [12].

While the primary objective of the BNL Muon $(g-2)$ experiment [13–18] was to measure the anomalous magnetic dipole moment of the muon, a_μ, this paper describes how, as a secondary measurement, a new limit on the electric dipole moment of the muon is obtained, a factor of 5 improvement over that achieved by the CERN experiment. The improved limit is interesting in its own right and helps to resolve one ambiguity in interpreting the difference between the theoretical and measured values of a_μ.

In general, the electric dipole moment, $\vec{d}$, and magnetic dipole moment (MDM, $\vec{\mu}$) are given by

$$\vec{d} = \eta \frac{q\hbar}{4mc} \vec{S}, \qquad \vec{\mu} = g \frac{q}{2m} \vec{s}, \tag{1}$$

where η describes the size of the EDM, $gq/(2m)$ is the gyromagnetic ratio, q and m are the particle's charge and mass, respectively, and $\vec{S}$ is a unit vector directed along $\vec{s}$, the true spin vector. For muons circulating in a storage ring, such as those used by both the CERN and BNL experiments, the spin vector's precession in the muon rest frame (MRF) depends on the interaction of its MDM with the magnetic field and of its EDM with the electric field. Measurements involving the former interaction can provide a determination of the magnetic anomaly, while those involving the latter can be used to determine the EDM. Note that if CPT symmetry is assumed, the η parameter is the same for positive and negative muons while $\vec{d}$ changes sign.

In the presence of electric and magnetic fields, in the laboratory frame of reference, the rate of spin precession relative to the muon momentum direction is given by the sum of contributions from the MDM and EDM: $\vec{\omega} = \vec{\omega}_a + \vec{\omega}_{\rm EDM}$, where, in the approximation $\vec{\beta} \cdot \vec{B} \approx 0$,

$$\vec{\omega}_a = -\frac{q}{m}\left[a_\mu \vec{B} + \left(-a_\mu + \frac{1}{\gamma^2 - 1}\right)\vec{\beta} \times \frac{\vec{E}}{c}\right]. \tag{2}$$

In the approximation $\vec{\beta} \cdot \vec{E} \approx 0$,

$$\vec{\omega}_{\rm EDM} = -\eta \frac{q}{2m}\left(\vec{\beta} \times \vec{B} + \frac{\vec{E}}{c}\right) = -\frac{\eta}{2mc}\vec{F}, \tag{3}$$

where q is the muon charge, $\vec{B}$ is the main dipole field and $\vec{E}$ is the field of the focusing electrostatic quadrupoles, $a_\mu = (g-2)/2 \approx 10^{-3}$ is the anomalous magnetic moment, and $\vec{F}$ is the Lorentz force. Here, ω_a, the $g-2$ precession frequency, includes contributions from both the Larmor and Thomas precessions. Both $\vec{F}$ and therefore $\vec{\omega}_{\rm EDM}$ are oriented along the radial direction while the magnetic field and therefore $\vec{\omega}_a$ are directed vertically. A nonzero EDM slightly tips the direction of $\vec{\omega}_a$ out of the vertical direction and slightly increases the precession frequency.

Under a Lorentz transformation, the laboratory magnetic field leads to a large electric as well as a magnetic field in the MRF. In fact, since the effect of the induced electric field, from $\vec{\beta} \times \vec{B}$, on $\vec{\omega}_{\rm EDM}$ is much larger than that produced by the focusing quadrupole field, the latter is ignored.

The BNL $(g-2)$ experiment and the earlier CERN [19,20] experiment were optimized to measure a_μ. Both experiments stored muons with the ''magic'' momentum $p \approx 3.094$ GeV/c, corresponding to $\gamma \approx 29.3$ and $\gamma\tau \approx 64.4$ μs, which gives $(\gamma^2 - 1)^{-1} - a_\mu \approx 0$. With this choice of beam momentum, the effect of the focusing electric field on $\vec{\omega}_a$ is zero. $\vec{\omega}_a$ is oriented vertically, parallel, or antiparallel to $\vec{B}$.

Both the MDM and EDM measurements rely on the detection of positrons or electrons from the three-body decays of the muons, $\mu^+ \to e^+ + \nu_e + \bar{\nu}_\mu$ or $\mu^- \to e^- + \bar{\nu}_e + \nu_\mu$. Positive muons were stored during the 1999 and 2000 data runs, while negative muons were stored in the 2001 data run. (Positrons will be used generically to refer to both electrons and positrons in the subsequent discussion.) The positron laboratory energies range from 0 to 3.1 GeV. All positrons with energies in excess of 1.2 GeV, which are the ones of interest here, are initially directed within approximately 40 mrad of the laboratory muon momentum direction. Most positrons have momenta that are less than those of the muons and are swept by the magnetic field to the inside of the storage ring, where they can be intercepted by the detector system.

A consequence of maximal parity violation in the muon decay is a large correlation between the direction of the positron momentum and the muon spin in the MRF. For

μ^+ (μ^-) decay, the positron (electron) momentum is preferentially directed parallel (antiparallel) to the spin.

Transforming to the laboratory frame, the number of positrons in a given energy range is modulated according to whether the polarization is along or opposite the direction of motion of the muon, following the familiar functional form

$$N(t) = N_0 e^{-\lambda t}(1 + A\cos(\omega t + \Phi)), \tag{4}$$

where $\tau_\mu = \gamma\tau_0 = \lambda^{-1}$ is the dilated muon lifetime. For the μ^+ (μ^-), $N(t)$ is a maximum when the muon polarization is parallel (antiparallel) to the muon momentum. The observed value of ω is used to deduce a_μ, under the assumption that the effect of the EDM on the magnitude of the spin precession can be neglected. See the discussion associated with Eq. (16).

For a uniform B field and in the absence of an EDM, all muon spins would precess at the same rate, regardless of trajectory or momentum, except for very small corrections for betatron motion and for the effect of the electric field on those muons whose momenta are not precisely magic. The precession vector $\vec{\omega}$ would be antiparallel to the vertical magnetic field or, equivalently, the spin vectors would precess in the horizontal plane. To investigate the implications of a nonzero EDM, the detector acceptance and spin motion are described in more detail.

The five-parameter equation for $N(t)$, Eq. (4), can be rewritten in the more general (differential) form, using MRF coordinates

$$P(\alpha, \tilde{\theta}, \tilde{\phi}, t)d\alpha d\tilde{\Omega} = n(\alpha)[1 + a(\alpha)\hat{\tilde{p}} \cdot \hat{s}(t)]d\alpha d\tilde{\Omega}, \tag{5}$$

where $\alpha = (E/E_{\max})^{\mathrm{MRF}}$, the fractional positron decay energy in the MRF, $\hat{\tilde{p}}$ is a unit vector along the decay positron's momentum, $\hat{s}$ is the muon spin, and a is the decay asymmetry. The tildes refer to MRF coordinates: $\hat{\tilde{x}}$ points in the outward radial direction, $\hat{\tilde{y}}$ points upward, and $\hat{\tilde{z}}$ lies along the muon momentum. The corresponding polar and azimuthal angles are denoted $\tilde{\theta}$ and $\tilde{\phi}$, respectively. The decay asymmetry is given by the expression

$$a(\alpha) = \frac{2\alpha - 1}{3 - 2\alpha}. \tag{6}$$

Alternatively, in integral form, we have

$$N(t) = N_0 e^{-\lambda t}(1 + \vec{A} \cdot \vec{s}(t)), \tag{7}$$

where $\vec{s}$ is the precessing polarization vector of the muon ensemble, $\vec{A}$ is the average *asymmetry vector*, the average of $a\hat{\tilde{p}}$ over detected decays. Of course, the asymmetry vector of a data sample depends on the MRF energies and angles of *accepted* positrons. For example, if positrons were only accepted if they struck detectors above (below) the storage ring midplane, then $\vec{A}$ would acquire a positive (negative) vertical component.

In Eq. (7), $\vec{s}(t)$ describes the spin motion. $\vec{A}$ includes the effects of the weak decay on the electron distribution, as well as detector acceptance. Consider the a_μ measurement. We define a local, lab-frame, Cartesian coordinate system where $\hat{x}$ and $\hat{y}$ are directed radially outward and vertically up, respectively, and $\hat{z}$ is longitudinal, along the motion of the stored muon beam. For the a_μ analysis, there is no bias in the spectra of positrons selected, above or below the midplane, and therefore $A_y \approx 0$. Moreover, there is little detector bias for positrons with negative versus positive radial momentum components. Thus $A_x \approx 0$. The preferential selection of positrons with high laboratory frame energies results in a large value of A_z. Therefore $\vec{A} \approx A_z\hat{z}$, with $\hat{z}$ longitudinal and Eq. (7) reduces to Eq. (4).

For a lab-frame decay electron energy fraction $f = E/E_{\max}$, A_z is given by

$$A_z = \frac{8f^2 - f - 1}{5 + 5f - 4f^2}, \tag{8}$$

with a corresponding (relative) number of muons

$$N = \frac{2(1 - f)(5 + 5f - 4f^2)}{12\pi}, \tag{9}$$

ignoring the effect of detector acceptance. The magnetic anomaly a_μ is derived from the experimentally determined value of ω. The statistical uncertainty on ω in Eq. (4) is inversely proportional to $(N_0A_0^2)^{1/2}$, where N_0 and A_0 refer to the ensemble of accepted events. Graphs of differential A (or A_z, strictly speaking), N, and NA^2 vs f, the last a statistical figure of merit (FOM), are shown in Fig. 1. Imposing an energy threshold selects a subset of decay positrons with a net average longitudinal momentum in the MRF, which leads to the oscillation in $N(t)$.

The asymmetry vector formalism can also be used in the context of the EDM analysis. The asymmetry for decays

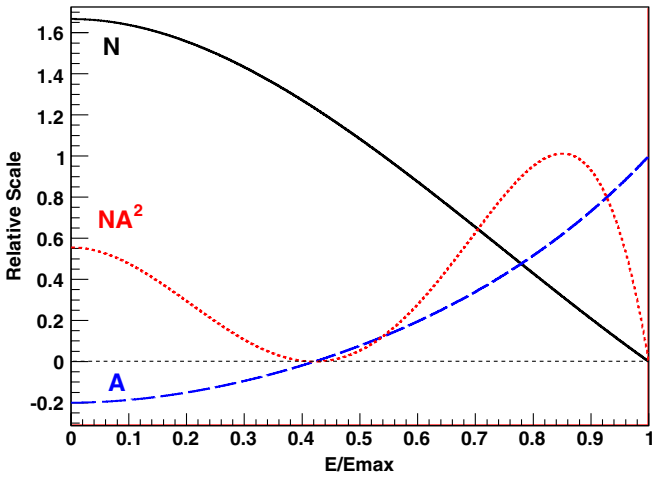

FIG. 1 (color online). Number N (solid line), $g - 2$ differential asymmetry A (dashed line), and $g - 2$ statistical figure of merit (FOM, dotted line) NA^2 vs laboratory frame energy fraction.

selected along any direction u in the transverse (x, y) plane is given by

$$A_u = \cos\phi \frac{8(1+4f)\sqrt{(1-f)f}}{5(5+5f-4f^2)}, \tag{10}$$

where $\tan\phi = p_y/p_x$, with p_x and p_y the transverse momenta and ϕ the azimuthal angle. The corresponding asymmetry, A_u, and differential statistical figure of merit, NA_u^2, are shown in Fig. 2. The sensitivity to an EDM is greatest over a broad range of lab energies, for 0.2 to 0.7 of the maximum.

Concerning the spin motion, with no EDM, the only significant torque is that produced by the interaction of the magnetic moment with the magnetic field. The spin vector precesses in the $x-z$ plane relative to the momentum vector according to $\vec{\omega}_a = -a_\mu(q/m)\vec{B}$. For μ^+, the polarization vector as a function of time is given by

$$\vec{s}(t) = -s_\perp \sin(\omega t + \Phi)\hat{x} - s_\parallel \hat{y} + s_\perp \cos(\omega t + \Phi)\hat{z}, \tag{11}$$

where $s_\parallel$ and $s_\perp$ are, respectively, the magnitudes of the components parallel and perpendicular to $\vec{\omega}$.

With a nonzero EDM, the precession is no longer confined to the horizontal plane. When the torque due to the motional electric field acting on an EDM is included, there is an additional spin precession $\vec{\omega}_{\rm EDM} = -(\eta/2) \times (q/m)\vec{\beta} \times \vec{B}$, which is directed radially in the storage ring. The plane of spin precession, which is perpendicular to the total precession vector $\vec{\omega} = \vec{\omega}_a + \vec{\omega}_{\rm EDM}$, is tipped out of the orbit plane by an angle

$$\delta = \tan^{-1}[\eta\beta/(2a_\mu)], \tag{12}$$

where a_μ is the anomaly and we see that δ is approximately proportional to the magnitude of the EDM. The spin precession is now given by

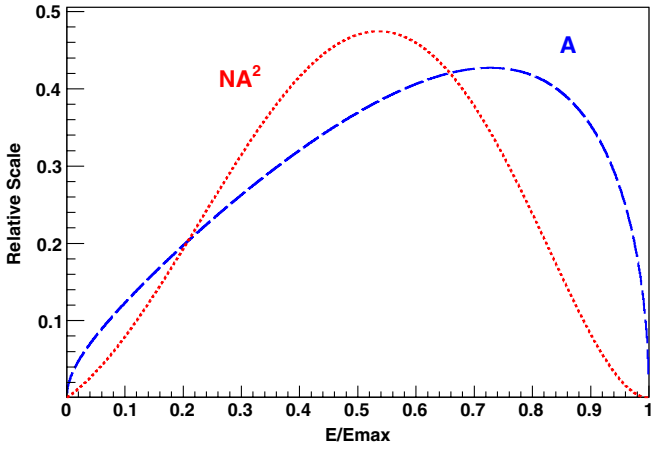

FIG. 2 (color online). Differential EDM asymmetry, A_u (dashed line), and statistical figure of merit, NA_u^2 (dotted line), vs laboratory frame energy fraction.

$$\vec{s}(t) = (-s_\perp \cos\delta \sin(\omega t + \Phi) + s_\parallel \sin\delta)\hat{x} - (s_\parallel \cos\delta + s_\perp \sin\delta \sin(\omega t + \Phi))\hat{y} + s_\perp \cos(\omega t + \Phi)\hat{z}, \tag{13}$$

that is, the average vertical component of the spin polarization oscillates at angular frequency ω, with an amplitude which is proportional to the EDM. The parallel and perpendicular components are defined with respect to the new direction of $\vec{\omega}$. If s_{y0} represents the vertical component of the beam's polarization at injection, which in the $g-2$ experiment is very small, the maximum excursion $|s_y - s_{y0}|$ occurs when the polarization is directed either along or opposite to the radial direction. To be precise, the vertical EDM oscillation leads the $(g-2)$ oscillation in $N(t)$ by 90°. This phase difference, which is the same for positive and negative muons, is useful in suppressing false EDM signals, as discussed below. It is also important to note that the phenomenology of the EDM-related spin motion is charge independent—if η is the same for positive and negative muons, the tipping of the precession plane, and the small change in frequency are identical.

If the asymmetry term in Eq. (5) is given the explicit form

$$a(f,\theta)\hat{p}(f,\theta,\phi) = A_{xy}(f,\theta)\cos\phi\hat{x} + A_{xy}(f,\theta)\sin\phi\hat{y} + A_z(f,\theta)\hat{z}, \tag{14}$$

using lab-frame variables f and θ, the corresponding dot product takes the form

$$\begin{aligned} a(f,\theta)\hat{p}(f,\theta,\phi)\cdot\hat{s}(t) &= A_z(f,\theta)(s_\perp\cos(\omega t+\Phi)) \\ &\quad + A_{xy}(f,\theta)\cos\phi(-s_\perp\cos\delta\sin(\omega t+\Phi) \\ &\quad + s_\parallel\sin\delta) + A_{xy}(f,\theta)\sin\phi(-s_\parallel\cos\delta - s_\perp \\ &\quad \times \sin\delta\sin(\omega t+\Phi)). \end{aligned} \tag{15}$$

The first term on the right-hand side, which arises from the longitudinal component of the asymmetry vector, has the $\cos(\omega t + \Phi)$ time dependence characteristic of the anomalous precession. The second (radial asymmetry) term, receives a contribution from the EDM, but is not readily observable because it cannot be distinguished from a small shift in the oscillation phase angle. The third (vertical asymmetry) term has the sought-for vertical oscillation, with an amplitude proportional to the EDM.

As noted above, a nonzero EDM increases the total spin precession frequency

$$\omega = \omega_a\sqrt{1+\tan^2\delta}. \tag{16}$$

While the roughly 3 standard deviation difference between the measured and theoretically predicted values of a_μ [18] could be the result of new physics such as supersymmetry or muon substructure, it could also be caused by a shift in

the value of ω_a produced by a nonzero EDM; see Eqs. (2), (3), and (16). A sufficiently precise measurement of the muon EDM could help resolve this ambiguity.

II. EXPERIMENTAL APPARATUS

Details on the $g-2$ storage ring [21], detectors [22,23], and on the anomalous precession analysis are presented elsewhere [13–18]. The storage ring magnet is 44 m in circumference with a dipole field of 1.45 T. A plan view of the storage ring and detectors is shown in Fig. 3. Muons are injected nearly tangent to the circumference through the field-free region provided by a superconducting inflector. The beam is centered on the storage region by means of a small magnetic kick applied at 90° downstream from the inflector. Data used in the anomalous precession and EDM analyses are collected for more than ten muon lifetimes during each injection cycle. While the details of beam injection and magnet design were rather different, the layout of the CERN III storage ring and detectors were very similar to those of E821.

III. MEASURING THE EDM

The measurement of the muon EDM requires the detection of oscillations in p_y, the vertical momentum of the decay positrons, which reflect the oscillations in s_y, the vertical polarization of the muon beam. The amplitude of the oscillations is proportional to the EDM. A measurement of the average vertical decay angle vs time, which picks out the third term on the right-hand side of Eq. (15), provides the most direct indication of possible oscillations in s_y.

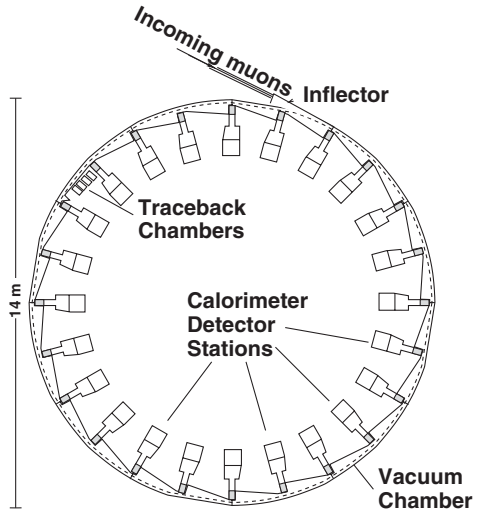

FIG. 3. A plan view of the $g-2$ storage ring showing the positions of the 24 calorimeters, the traceback chambers, and other devices. The calorimeters are numbered 1–24 starting from the injection point and proceeding clockwise.

In order to optimize the experimental sensitivity to a nonzero EDM, the range of positron energies should maximize the FOM for oscillations in s_y (see Fig. 2) and maximize $s_\perp$. Naturally, the beam polarization is optimized for the $g-2$ measurement. The EDM FOM varies slowly with positron energy—a broad range of energies around 1.5 GeV is acceptable. It is important to note, however, that the acceptances of the $(g-2)$ detector systems are not optimized for the EDM measurement. Those acceptances generally rise with increasing positron energy, reach a maximum near 2.8 GeV, and then fall to the energy end point at 3.1 GeV.

If direct tracking measurements are unavailable (as was the case in the CERN III experiment), the observation of certain rate oscillations with a $\sin(\omega t+\Phi)$ time dependence [see Eq. (15)] can be used instead. In this case, one should select data subsets with nonzero average positron momentum along y, in order to maximize $|A_y|$. In practice, this means selecting decay positron hits either above or below the storage ring midplane. A further refinement is to measure the oscillation phase as a function of vertical position on a detector. The $\sin(\omega t+\Phi)$ time dependence of the vertical oscillation is shifted by 90° relative to the $g-2$ precession [$\cos(\omega t+\Phi)$] and the $\sin\phi$ factor in the last term provides a sign flip between the signals observed above or below the storage ring midplane. In both these approaches, the correlation of detected vertical position to vertical angle, while strong, is reduced somewhat by the range of vertical decay positions.

The CERN III experiment [6] mounted two adjacent scintillator paddles on the entrance face (where most positrons enter) of one of the calorimeters. One paddle was mounted above the vertical midplane of the calorimeter, and the other below. An event was counted when a signal from a paddle was registered in coincidence with a calorimeter signal that exceeded a specified energy threshold, typically 1.2–1.4 GeV. Any oscillation in $\langle p_y\rangle$ would cause a corresponding oscillation in the ratio of the sum and difference of count rates in the up (N^+) and down (N^-) paddles,

$$r(t)=\frac{N^+(t)-N^-(t)}{N^+(t)+N^-(t)}. \tag{17}$$

In the presence of an EDM but in the absence of field perturbations which could bend decay electron tracks, expressions for N^+ and N^- can be written in terms of the asymmetry vector for each data sample. A subsample of decay positrons which are detected above the orbit plane will have a nonzero vertical asymmetry component, $\vec{A}^+ = A_y\hat{y}+A_z\hat{z}$. Similarly a subsample below the orbit plane will have $\vec{A}^- = -A_y\hat{y}+A_z\hat{z}$. Assuming the gain and acceptance of the upper and lower detectors are equal and the storage ring and vertical detector midplane are identical, Eqs. (7) and (13) with $s_\parallel = 0$ give

$$N^{\pm} = \tfrac{1}{2}N_0 e^{-\lambda t}(1 \mp A_y s_\perp \sin\delta \sin(\omega t + \Phi) + A_z s_\perp \cos(\omega t + \Phi)). \quad (18)$$

As expected, the term containing A_y is proportional to the EDM, oscillates at angular frequency ω, and is 90° out of phase with the ordinary $g - 2$ precession given by the term containing A_z.

Separating out the contribution from the EDM, the expression for $N^{\pm}$ becomes

$$N^{\pm} = \tfrac{1}{2}N_0 e^{-\lambda t}[1 \mp A_{\rm EDM} \sin(\omega t + \Phi) + A_\mu \cos(\omega t + \Phi)], \quad (19)$$

where $A_{\rm EDM} = A_y s_\perp \sin\delta$ is proportional to d_μ and $A_\mu = A_z s_\perp$.

Equivalently one can define an angle $\Psi = \tan^{-1}(-A_{\rm EDM}/A_\mu)$ and an overall asymmetry $A = \sqrt{A_\mu^2 + A_{\rm EDM}^2}$ and write

$$N^{\pm} = \tfrac{1}{2}N_0 e^{-\lambda t}[1 + A\cos(\omega t + \Phi \pm \Psi)]. \quad (20)$$

In the presence of an EDM only (again, without field perturbations), d_μ can be obtained from either a fit to the ratio, Eq. (17),

$$r(t) = \frac{A_{\rm EDM}\sin(\omega t + \Phi)}{1 + A_\mu \cos(\omega t + \Phi)}, \quad (21)$$

or from separate fits of Eq. (20) to the data from the top and bottom paddles, with the EDM being inferred from the magnitude of angle Ψ. The latter approach is better, since many small spin perturbations, for example, from spin resonances, change $N^+ - N^-$ in Eq. (21) without changing Ψ in Eq. (20). Spin resonances, however, are very weak in the $g - 2$ storage ring. Only high longitudinal modes of some nonlinear field components can oscillate, in the MRF, in resonance with spin precession. For such resonances, the original constant part of the vertical spin component changes slowly.

Use of the latter approach led to the CERN result [6] on the combined μ^+ and μ^- EDMs, $d_\mu = (-3.7 \pm 3.4) \times 10^{-19} e$ cm. Contrary to the sign convention in Bailey *et al.*, we choose to cite the EDM for the negative muon rather than for the positive muon, after combining the results for the negative and positive muon, assuming *CPT*. This is consistent with zero, giving $d_\mu < 1.05 \times 10^{-18} e$ cm at the 95% confidence level. The overall uncertainty is evenly split between statistical and systematic errors.

The systematic error arises mainly from the uncertainty in the alignment of the detectors relative to the muon beam, which, coupled with the spin precession, can produce a false EDM signal. Along the trajectory from the muon decay point to the detector, positrons emitted with outward radial momentum components will travel farther than those with inward components, and will therefore have more time to spread out in the vertical direction. When the muon spin is pointing radially outward, more positrons are emitted with outward radial momentum components than inward, and the width of the vertical distribution of positrons at the detector entrance face will be larger than when the spin is pointing radially inward. The width of the vertical distribution of positrons therefore ''breathes'' at the spin precession frequency $\omega/(2\pi)$.

Ideally, the average distribution of the muons in the vertical coordinate is symmetric about $y = 0$, and this symmetry is generally reflected in the decay positrons observed by the detectors. Indeed, if the EDM is zero, if the initial vertical component of the spin polarization is zero, if the vertical position of the dividing line between scintillator paddles is aligned with $y = 0$, and if the paddles have the same efficiency of positron detection, then the vertical distribution of detected positrons is symmetric in y at all times and $r(t) = 0$. If any of these requirements are not met, then the time average value of $r(t)$, $\langle r(t)\rangle$, will be nonzero in general. A nonzero $\langle r(t)\rangle$ is not, by itself, significant. However, the breathing of the vertical width of the beam will now introduce oscillations in $r(t)$ at frequency $\omega/(2\pi)$, *in phase with the oscillations that would be produced by a true EDM*. In other words, it would produce a false EDM signal.

Corrections for detector inefficiency and misalignment can be made, using knowledge of the shape of the vertical distribution as a function of time, the acceptance of the paddles as a function of time, the value of s_{y0}, and the measured value of $\langle r(t)\rangle$. However, in the case of the CERN III experiment, which had only two paddles mounted on a single calorimeter, detailed measurements of the vertical distribution could not be made. In E821, there is more information on the vertical distribution because the detectors have more than twofold vertical segmentation. However, the relative acceptances of the elements are more complicated because they depend not only on the efficiency of the scintillators but also on the gain stability and relative efficiency, versus time, of the top half of the calorimeter relative to the bottom. The time dependence of the vertical distribution on the detector face is readily simulated, but not the detector response, which must take into account the time-varying energy and incident angles of the positrons, as well as geometric variations in gain and efficiency of the scintillator and calorimeter. Limitations on the corrections cause these alignment effects to dominate the systematic error.

IV. THE BNL EDM MEASUREMENTS

In addition to the positron calorimeters, three kinds of detectors were used to measure the EDM in the BNL experiment:

(i) The front scintillation detectors (FSD) are used to measure any oscillation in the average vertical position of the decay positrons as they enter the calorimeters. They consist of an array of five horizontal

scintillator paddles which cover the entrance faces of roughly half the calorimeters [22]; see Figs. 3 and 4. About 10 of the FSDs were instrumented, typically those mounted on calorimeters where the injection-related background was the least severe. The increased segmentation over the CERN arrangement helps improve knowledge of the vertical distribution of the positrons, thereby reducing the misalignment error, and permits the more sophisticated analysis which is described below.

(ii) The position sensitive detectors (PSDs) [23] are a much more finely segmented version of the FSD, with horizontal as well as vertical segmentation. They cover the positron entrance faces of calorimeters 13, 14, 15, 18, and 24.

(iii) The traceback wire chamber (TWC) system consists of a series of drift chambers mounted in front of calorimeter 20, along the path of the incoming decay positrons; see Fig. 5. The TWCs are used to measure the pitch angle of the decay positrons. They also provide information on the phase space distribution of the muons in the storage ring. Tracks measured by the traceback system are extrapolated back into the storage volume, to the position where the momentum points tangent to the storage ring, which is a good approximation to the point of decay.

Another difference between the CERN III and BNL EDM measurements concerns the stored beam. The functions which describe the time spectra [Eq. (7), for example] are constructed with the assumption that while the muons themselves are moving, the spatial distribution is static. In fact, the muon beam arrives in a bunch, which provides a modulation of the decay signal with period 149.2 ns, the time it takes for the bunch to circle through the storage ring. This *fast rotation* signal, which is prominent for roughly the first 70 μs, was filtered out in both the CERN III and E821 analyses. However, because of our direct muon injection technique, there is another very important collective beam motion. For several hundreds of microseconds after injection, the stored muon beam exhibits a variety of coherent betatron oscillations collectively referred to as CBO. Among these is an oscillation in the radial beam position (measured at a fixed point in the ring) at frequency $f_{\mathrm{CBO}} \approx 465$ kHz [18]. Descriptions of the vertical distributions of positrons on detector faces must account for beam motion. When the beam radius is larger than average, the width of the vertical distribution of positrons at the detector is larger because of the longer distance traveled, and conversely, when the beam radius is smaller than average, the vertical width is smaller.

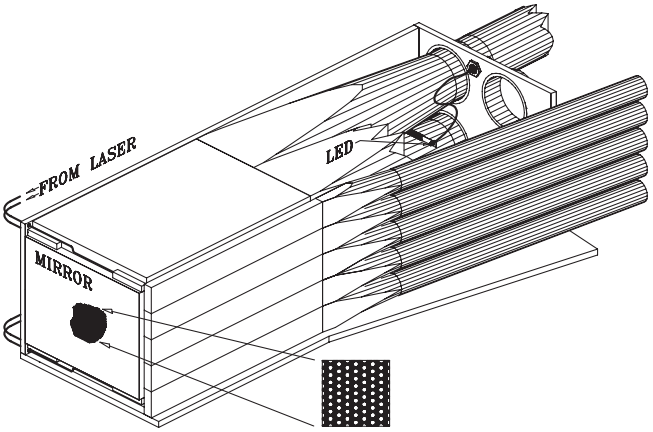

FIG. 4. Detailed view of a detector station. The calorimeter consists of scintillating fibers embedded in a lead-epoxy matrix, with the fibers being directed radially in the storage ring. Five horizontal scintillators, the FSD segments, cover the positron entrance face of the calorimeter. Each calorimeter is approximately 23 cm (wide) by 14 cm (high) by 15 cm (deep). The PSD (not shown) is placed in front of the FSD.

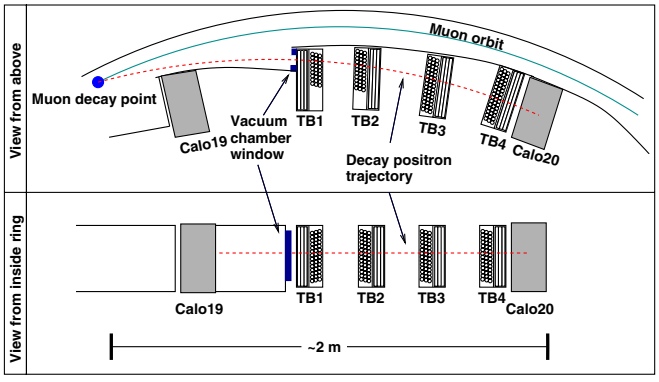

FIG. 5 (color online). Top and side views (not to scale) of the traceback system. Muons decay to positrons in the storage region. The positron then must travel through the thin window in the vacuum chamber scallop, through the traceback chambers, and into the calorimeter. Horizontally lying straw chambers allow the precise reconstruction of the vertical angle of the positron.

Combined with a detector-beam misalignment, radial beam motion can produce the same sort of vertical oscillation in $\langle p_y \rangle$ as the anomalous precession of the spin, again proportional to the magnitude of the misalignment. However, because the CBO-induced frequency is different from that produced by an EDM, this oscillation will not be mistaken for an EDM signal, but instead can be used to calibrate, and ultimately to correct, the misalignment error.

While the FSD and PSD provide EDM measurements patterned on that of the CERN III experiment, the PSD provides another, qualitatively different, approach. The phase parameter Φ in Eq. (4), varies with y, the detector vertical position. As explained earlier, for decays in which the polarization points outward, the ensemble of decay positrons spreads out more in the vertical direction than when the polarization points inward. As a consequence, positrons detected far away from the vertical midplane ($|y|$ large) will be more likely to come from outward decays than from inward decays. Conversely, inward decays will

be more likely than outward decays when $|y|$ is small. Therefore Φ will depend slightly on y. If $d_\mu = 0$, the spin precesses in the horizontal plane, and $\Phi(y)$ will be symmetric in y. However, if $d_\mu \neq 0$, the plane of the spin precession is tipped out of the horizontal plane, and $\Phi(y)$ will *not* be symmetric in y.

Finally, although the TWCs were originally designed to determine the phase space of the stored muons, for use in the anomalous precession analysis, their measurement of the average vertical decay angle provides an independent measurement of d_μ, one which is largely immune to the detector misalignment problem. In the absence of radial magnetic fields, the vertical angle of the track as measured in the traceback system, is the same as that at the moment of decay. A nonzero EDM would be reflected in an oscillation of the vertical component of the positron momentum, 90° out of phase with the $(g-2)$ number oscillation. Further details on the EDM measurements made with these three detectors are presented in the following sections.

V. TRACEBACK ANALYSIS OF 1999 AND 2000 μ^+ DATA SETS

A. The traceback detector

The traceback detector consists of a set of eight, three-layer drift tube planes, designed to measure positron trajectories along their usual decay path out from the storage volume into the calorimeters. This detector was installed during the 1999 and 2000 running periods at a single position in the ring. By analyzing the positron drift time spectrum in a straw, the radius from the anode wire at which the particle passed is determined. Tracks are fit to these drift circles according to the equations of motion of a charged particle in a magnetic field. Because of the very inhomogeneous magnetic field in the region of the traceback detector (10 T/m), tracks must be integrated with a very small step size. The relatively high precision of the track reconstruction offers a detailed, time-varying picture of the decay positron trajectories and the stored muon beam. In particular, for the positron's vertical angle of entrance into the detector, which is examined for an EDM oscillation signal, the resolution is approximately 350 μrad.

B. Traceback analysis description and results

As indicated above, a nonzero EDM would generate an oscillation in the vertical angle of decay positrons, 90° out of phase with the $g-2$ number modulation, $N(t)$. While there are several mechanisms which might generate oscillations in the measured vertical angle, all are in phase with the number oscillation, $N(t)$, and this is also measured in the traceback system. By fixing the relative phase of the EDM and $N(t)$ oscillations, the false EDM signals produced by these effects can be minimized.

The $N(t)$ spectrum is fit first. To minimize the effect of periodic disturbances at other frequencies, which dephase and average away when many time bins are combined, the data are plotted vs time, modulo the $g-2$ precession period. The spectrum is fit to Eq. (22) where the precession period $T = 2\pi/\omega = 4365.4$ ns is fixed by the result of the anomalous precession analysis,

$$N(t) = e^{-t/\tau_e}(N_0 + W\cos(\omega t + \Phi)), \tag{22}$$

where τ_e is an empirical term which parametrizes both the effect of muon decay and that of the recovery of the chambers, which are disabled during injection. The phase is determined to better than 3 mrad (see Fig. 6).

Once the precession phase is established, a plot of average vertical angle versus time, modulo the $g-2$ precession period, is fit to the function

$$\theta(t) = M + A_\mu\cos(\omega t + \Phi) + A_{\mathrm{EDM}}\sin(\omega t + \Phi), \tag{23}$$

where ω remains fixed as before and Φ is set by the previous fit. The amplitude of the sine term represents the EDM signal.

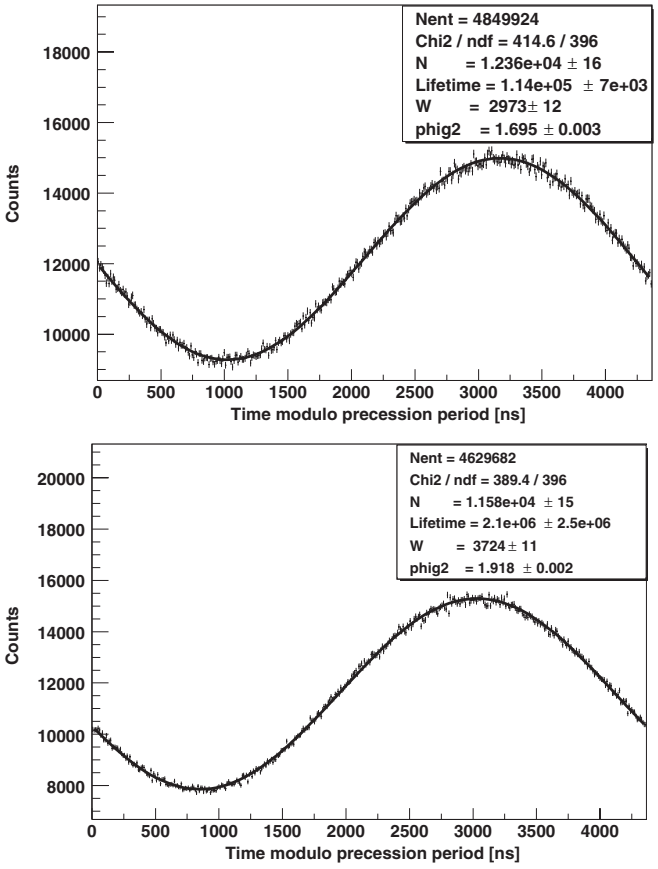

FIG. 6. Traceback analysis: Plots of the data and fits to Eq. (4), modulo the anomalous precession period, for each running period, as recorded by the traceback system (1999 top panel, 2000 bottom panel). The $g-2$ phase parameter (labeled phig2 in the fit box) is used in subsequent vertical angle fits.

The measurement of the vertical angle in the lab frame must be converted to a precession plane tilt angle in the muon rest frame [see Eq. (12)]. The conversion factor is determined through simulation. Several sets of simulated trajectories were generated and reconstructed, each having a different value for precession plane tilt. Shown in Fig. 7 is the fit EDM amplitude for various input precession plane tilts. A 3 μrad amplitude vertical oscillation is generated for each milliradian of precession plane tilt.

The 1999 and 2000 data sets contain, respectively, approximately 4.8×10^6 and 4.6×10^6 well-fit tracks. In each data set, approximately 15% of the tracks are background: misconstructed tracks or tracks scattered from the upstream vacuum chamber or previous calorimeter stations. To reduce the level of misconstructed tracks to the percent level requires cuts which would throw away most of the data. The more liberal cuts chosen for the final data sample do not induce a false EDM signal. The time spectrum of the average vertical angle combined into one histogram with a length of the precession period is then fit with the sum of a sine and cosine, as described above. Fits for each data set are shown in Figs. 8. The results are $(4.4 \pm 6.3) \times 10^{-6}$ rad oscillation for the 1999 data set and $(-4.5 \pm 6.2) \times 10^{-6}$ rad for the 2000 data set. Combining the results, an oscillation amplitude of $(-0.1 \pm 4.4) \times 10^{-6}$ rad is obtained, where the error is statistical.

Many systematic uncertainties have been studied and those relevant to the measurement are listed in Table II. The "radial field" error refers to the fact that an average radial magnetic field around the ring would tilt the precession plane in the same way as an EDM. The effect of a radial magnetic field on the decay positrons, which would change the vertical angle of the tracks, can be neglected. Another uncertainty comes from the geometry of the de-

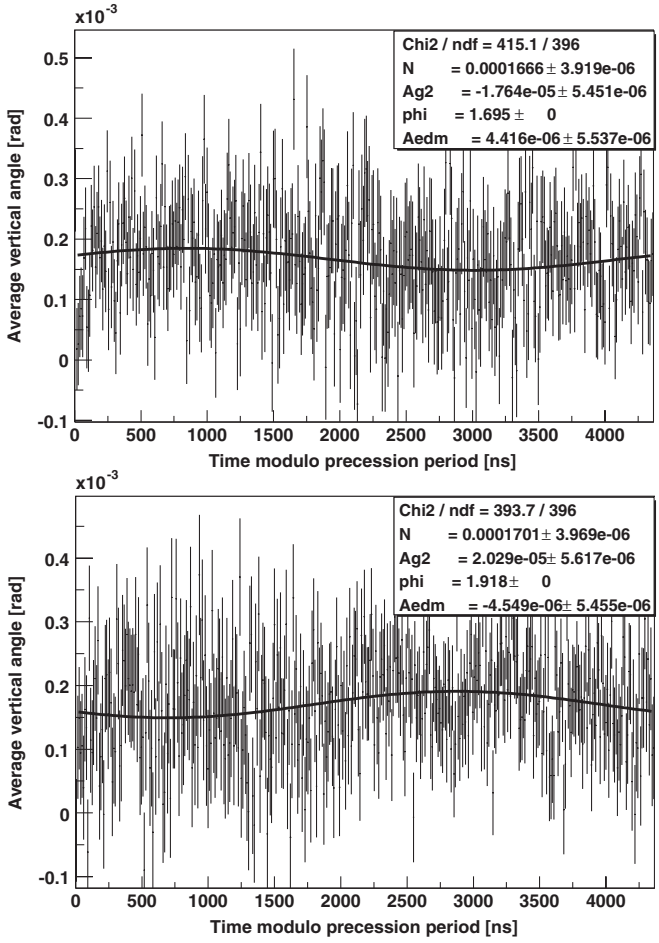

FIG. 8. Traceback analysis: Average vertical angle vs time, modulo the anomalous precession period, measured by the traceback system for each running period (1999 top panel, 2000 bottom panel). The data are fit to Eq. (23). The amplitude of the oscillations, A_{EDM}, is proportional to the EDM.

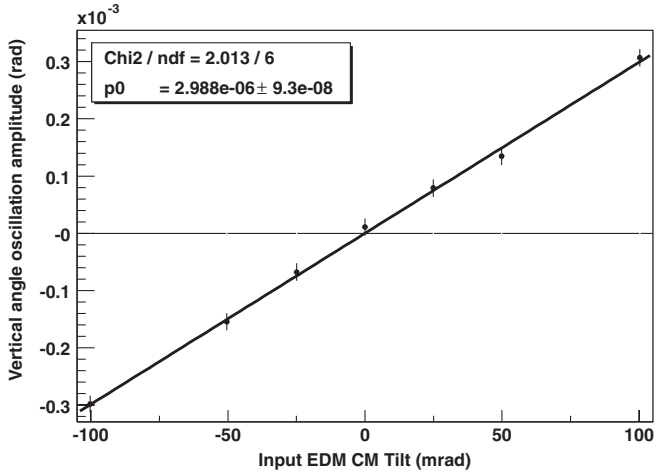

FIG. 7. Traceback EDM fit amplitude vs simulated input precession plane tilts. The fit function is a strict proportionality: the slope is parameter p_0 with no constant term. A vertical oscillation with amplitude 3×10^{-6} rad corresponds to 1×10^{-3} rad of precession plane tilt.

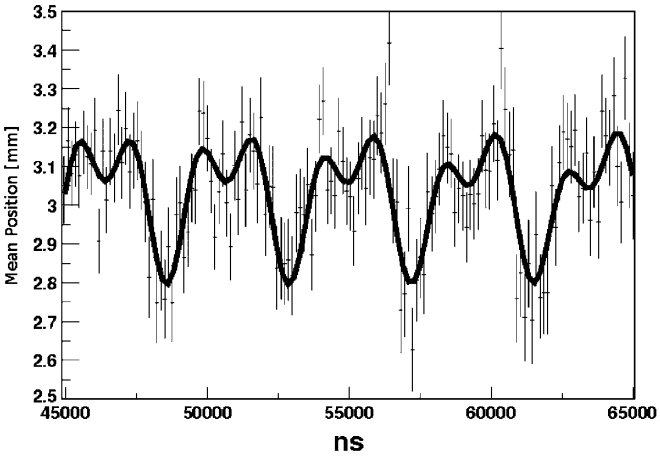

FIG. 9. Sample plot of the mean position on an FSD versus time in fill with fit to Eq. (25) overlaid. Oscillations at the $g - 2$ ($T \approx 4365$ ns) and CBO ($T \approx 2150$ ns) frequencies are visible. The 3 mm vertical offset was later corrected (see Figs. 10 and 11).

TABLE II. Table of systematic errors from the traceback analysis.

Systematic error	Vertical oscillation amplitude (μ rad lab)	Precession plane tilt (mrad)	False EDM generated 10^{-19} (e cm)
Radial field	0.13	0.04	0.045
Acceptance coupling	0.3	0.09	0.1
Horizontal CBO	0.3	0.09	0.1
No. oscillation phase fit	0.01	0.003	0.0034
Precession period	0.01	0.003	0.0034
Totals	0.44	0.13	0.14

tector. In making their way to the detectors, positrons with an initial outward radial momentum component travel farther, on average, than those with an initial inward radial momentum component. Combined with varying vertical angle acceptance for different decay azimuths and an off-center muon distribution, a radial beam oscillation can appear in the detector data as a vertical oscillation. An error on the number oscillation phase or period may result in some mixing between the number oscillation signal and the precession plane tilt signal. The total systematic error is 0.14×10^{-19} (e cm). For more details see [24]. The negligible systematic errors indicate that the TWC method should be considered in any future attempt to measure the muon EDM.

Since the systematic errors are negligible, the traceback system's measurement of the EDM for the positive muon is determined by the value and (statistical) error for the vertical oscillation amplitude alone: $(-0.04 \pm 1.6) \times 10^{-19}$ (e cm), which corresponds to an upper limit of

$$|d_{\mu^+}| < 3.2 \times 10^{-19}\ (e\,\mathrm{cm})\ (95\%\ \mathrm{C.L.}). \qquad (24)$$

VI. FSD ANALYSIS OF THE YEAR 2000 μ^+ DATA SET

As described in the Introduction, a nonzero EDM would result in an oscillation of the mean vertical position at the $g-2$ frequency but 90° out of phase with the number oscillation. Therefore, for each detector, the mean position of hits on the FSD, matched to calorimeter events with energy 1.4–3.2 GeV, is plotted versus time. (The center tile is not used in the mean.) An example from a single station is shown in Fig. 9. The plot is fit to

$$\begin{aligned} f(t) = {} & K + [S_{g2}\sin(\omega t) + C_{g2}\cos(\omega t)] + e^{-(t/\tau_{\mathrm{CBO}})} \\ & \times [S_{\mathrm{CBO}}\sin(\omega_{\mathrm{CBO}}(t-t_0) + \Phi_{\mathrm{CBO}}) \\ & + C_{\mathrm{CBO}}\cos(\omega_{\mathrm{CBO}}(t-t_0) + \Phi_{\mathrm{CBO}})] + Me^{-(t/\tau_M)}. \end{aligned} \qquad (25)$$

The constant term K characterizes the vertical offset between the beam and the detector. There are sine and cosine terms of frequency ω with the phase fixed such that the cosine term is aligned with the number oscillation. Thus, an EDM signal would appear 90° out of phase, in the sine term (S_{g2}); ω is fixed to the frequency measured in the $g-2$ analysis. t_0 is an empirical term, fixed to 100 μs.

In addition, there is a sinusoidal term with the frequency of the CBO. Horizontal focusing causes the beam position near any detector to oscillate radially at $\omega_{\mathrm{CBO}} \approx 465$ kHz. The oscillation is prominent at early times, but dephasing causes its amplitude to decay with a lifetime $\tau_{\mathrm{CBO}} \approx 100$ μs. The CBO is clearly evident in a plot of the vertical profile width versus time. The frequency ω_{CBO}, lifetime τ_{CBO}, and phase Φ_{CBO} of the CBO are obtained from fits to the width. Those parameters are then fixed in the fit to the average position versus time, Eq. (25). The final term, with τ_M fixed to 60 μs, accounts for slow changes in detector response and possible pulse pileup effects, when two pulses arrive within the detector dead time.

Approximately two-thirds of the way through the year 2000 data run, the stored beam was moved downward by 2 mm to improve its alignment with the detectors. Figure 10 shows the fitted value of the EDM term (S_{g2}) versus station number before the alignment. The figure shows significant variations between detectors with an average of 0.087 mm, corresponding to an EDM nearly as large as the CERN limit. Figure 11 is a similar plot from data taken after the beam alignment. Although the ampli-

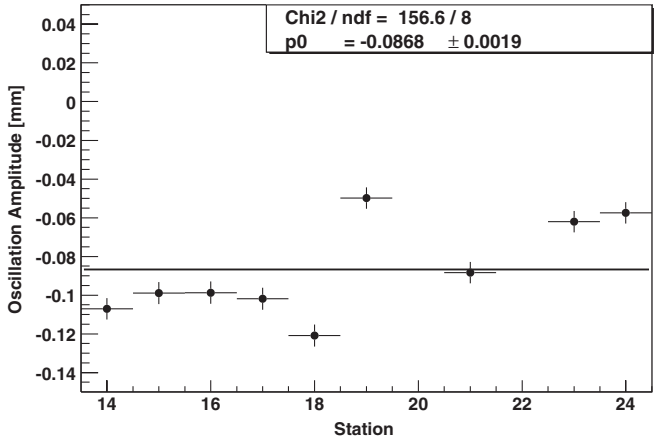

FIG. 10. FSD analysis: S_{g2} versus station before the beam realignment in the year 2000 data period. The offset from zero, indicated by fit parameter p_0, and inconsistencies between detectors indicated by the large χ^2 of the fit, are due to the misalignments between the detectors and the beam.

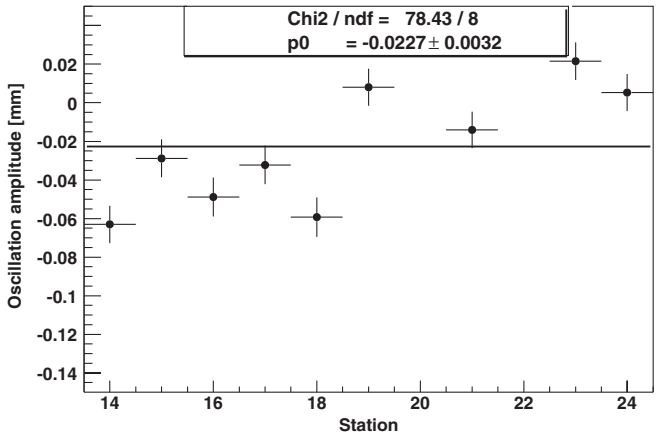

FIG. 11. FSD analysis: S_{g2} versus station after the beam realignment. The overall offset from zero is smaller when the beam is better aligned but the inconsistencies between detectors, indicated by a χ^2 which is only somewhat improved, remain. The line represents a best fit constant to the data.

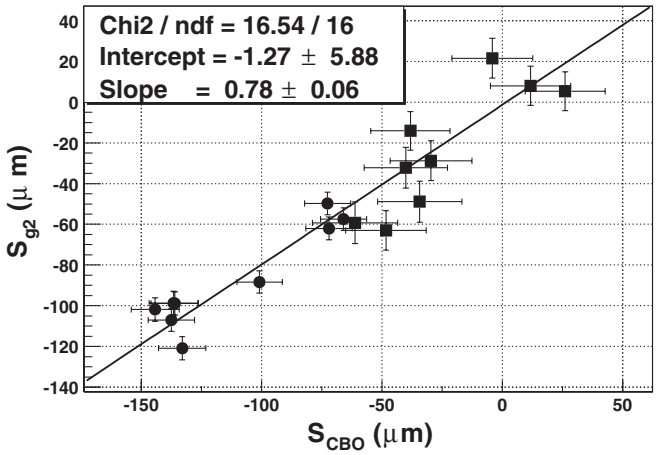

FIG. 12. FSD analysis: the $g-2$ sine amplitude vs CBO sine amplitude from fits to the mean vs time.

tudes of oscillation are much reduced after beam alignment, there are still unacceptably large variations among detectors.

As explained above, these inconsistencies arise from residual misalignment between the detectors and stored beam combined with oscillations in the width of the positron vertical profile at the $g-2$ frequency. While data taken after the beam was realigned show a significantly smaller oscillation, if the alignment were perfect and the EDM zero, there would be no oscillation at all. The amplitude of an oscillation caused by an EDM should be consistent from detector to detector.

The CBO oscillation that was described earlier can be used to eliminate the large false EDM signal that results from detector misalignment. The CBO causes an oscillation in the width of the vertical profile because, for example, decay positrons must travel farther to the detectors when the muons are at their maximum radial position. The oscillation in the mean vertical position at the CBO frequency results from the misalignment of the detector with the plane of the beam. Since the vertical oscillation at the CBO frequency is sensitive to the detector misalignment, it can be used to correct for the corresponding systematic error in the EDM measurement.

A plot of the vertical oscillation amplitude at the $g-2$ frequency (S_{g2}) versus the vertical oscillation amplitude at the CBO frequency (S_{CBO}) is shown in Fig. 12. The 18 points shown are data from the 9 FSDs used in the analysis before and after beam realignment. The fit to a line produces a good χ^2, showing, as indicated earlier, that the amplitudes of the two oscillations are well correlated. The y intercept, where the CBO oscillation disappears, corresponds to an EDM oscillation measurement made by a perfectly aligned detector, which thus eliminates a large systematic error.

From simulation, the expected vertical oscillation due to an EDM is 8.8 μm per 10^{-19} (e cm). The S_{g2} intercept,

$$S_{g2}(0) = (1.27 \pm 5.88)\ \mu\mathrm{m}, \tag{26}$$

implies an EDM measurement of

$$|d_{\mu^+}| < (0.14 \pm 0.67) \times 10^{-19}\ (e\,\mathrm{cm}), \tag{27}$$

using only the statistical error. A nearly identical relation between oscillation amplitude and EDM limit is obtained in the PSD analysis, presented below.

Systematic errors dominate the measurement. Any source of vertical oscillation at either the $g-2$ or CBO frequency, in the correct phase, is a potential source of systematic error. The largest of the errors is due to the tilt of the detectors. A tilt in the detector around the beam direction combined with a horizontal oscillation in the impact position on the detector face would result in an apparent vertical oscillation. Simulation studies of decay positron tracks reveal no horizontal oscillation on the detector face at the $g-2$ frequency in the EDM phase, but it does indicate a horizontal oscillation at the CBO frequency of amplitude 0.6 mm. Measurements with a level established that the average detector tilt was less than 8.7 mrad ($\frac{1}{2}°$), implying a systematic error of 6.1 μm on S_{g2}. A more direct measurement of detector tilt, which arrived at a much more stringent limit, was made with the PSD (see Sec. VII, below).

Another systematic error could arise if the electrostatic quadrupoles were themselves tilted with respect to the storage ring field. In this case, a small component of the nominally radial CBO oscillation frequency would be manifest as an oscillation in the vertical mean position of the decay positrons, even in a perfectly aligned detector. Surveys of the quadrupoles indicate a tilt of less than 2 mrad; the resulting systematic error is 3.9 μm.

If the average vertical spin component of the muon is not zero then neither is the average vertical angle of decay

positrons. Since there is a longer average path length for positrons emitted when the muon spin is outward than inward, this would result in an apparent vertical oscillation at the detector face, in phase with the expected EDM signal. The average vertical angle of positrons approaching a detector was measured by the traceback detector. The angle was combined with the change in path length for positrons from decays when the muon is pointed inward versus outward, obtained from simulation, to give an estimate of the vertical oscillation at the $g-2$ frequency due to muon vertical spin. This effect is also present at the CBO frequency since positrons from decays when the muons are farther out have longer path lengths to the detector. This leads to a partial cancellation of the systematic error, which is 5.1 μm, overall.

A radial magnetic field would deflect decay positrons vertically, causing a similar systematic error. Although the *average* radial field in the ring is known to be less than 20 ppm because it affects the beam position, the local radial magnetic field felt by the decay positrons may be larger than 100 ppm. The size of the error can be estimated in an analysis similar to that used for the muon vertical spin. Once again, the error of 2.5 μm reflects a partial cancellation from the CBO. It should be noted that the average part of the radial magnetic field affects the spin similarly to an EDM, thus changing the Ψ in Eq. (20). However, the radial field, which is only 20 ppm of the main vertical field, affects the spin at a level which is 2 orders of magnitude smaller than our experimental sensitivity to an EDM. The reason is that in spin dynamics, the average magnetic field effect is almost completely canceled by the average field of the focusing electrodes (while in beam dynamics, they cancel each other completely). And without an average radial magnetic field, the average electric field cannot appear in the $g-2$ storage ring with its homogeneous vertical magnetic field.

Since each of the top and bottom of the calorimeters is read out by a different photomultiplier tube, there is the potential for timing and energy calibration offsets. By applying different calibration constants to the top and bottom of each detector, the relative gains of the two halves were corrected to within 0.5%. The residual error results largely from the vertical offset of the beam during the year 2000 data-taking run. For the 2001 run, where the offset was much smaller, the corresponding error is about 0.1% (see Sec. VII). The timing difference was estimated using the cyclotron structure of the data seen early in each fill, before the beam debunches. The time at which the muon bunch passes each detector can be seen as a rate oscillation with a 149.2 ns period. By measuring the time of the peak of each bunch in the top and bottom of the calorimeter the average timing difference was found to be less than 0.5 ns. To determine the potential effects of these asymmetries, analyses were performed with offsets in the timing and calibration intentionally inserted. Based on these analyses, systematic errors due to timing and calibration offsets were estimated to be 3.2 and 2.8 μm, respectively.

TABLE III. FSD analysis: error table for S_{g2}, the EDM-sensitive parameter. The conversion to error on the EDM is $0.114 \times 10^{19}\ e\,\mathrm{cm}/\mu\mathrm{m}$.

Effect	Error (μm)
Detector tilt	6.1
Vertical spin	5.1
Quadrupole tilt	3.9
Timing offset	3.2
Energy calibration	2.8
Radial magnetic field	2.5
Albedo and doubles	2.0
Fitting method	1.0
Total systematic	10.4
Statistical	5.9
Total uncertainty	11.9

The sensitivity of the FSD tiles to low energy backscatter from the calorimeters (''albedo'') may also cause a systematic error. Albedo causes multiple tiles to fire at the same time, giving the appearance of two positrons hitting the detector when there was only one. Albedo is not a problem unless there is a difference in the sensitivity to albedo in the top and bottom of the detector. A limit on the size of this effect was determined by using several methods of dealing with apparent double hits (counting both, counting neither, counting one at random). No deviations in the results were found larger than 2.0 μm, which is taken to be the systematic error.

There are error bars on both abscissa and ordinate in Fig. 12. Our fits, which use an approximation for the latter error, introduce an additional systematic error of 1 μm. The effect of FSD tile inefficiency and dead time was also investigated but the resulting systematic errors were less than 1 μm and so were ignored.

The systematic effects, given in Table III, are uncorrelated; the uncertainties are added in quadrature. The total error is 11.9 μm, which gives an EDM measurement of

$$d_{\mu^+} = (-0.1 \pm 1.4) \times 10^{-19}\ (e\,\mathrm{cm}), \tag{28}$$

and a limit

$$|d_{\mu^+}| < 2.9 \times 10^{-19}\ (e\,\mathrm{cm})\ (95\%\ \mathrm{C.L.}). \tag{29}$$

VII. PSD ANALYSIS OF 2001 (μ^-) DATA

The PSD [23] is a finely segmented two-dimensional scintillator hodoscope covering the positron entrance faces of five detector stations. Each hodoscope consists of one plane of 20 scintillator tiles directed horizontally and one plane of 32 tiles directed vertically. Each tile is 8 mm wide and 7 mm thick. The PSDs were mounted on the face of the calorimeters, providing vertical and horizontal position

data. As indicated in the Introduction, two EDM searches were made with the PSD, one modeled on that made with the FSD and another in which the symmetry of Φ with y was examined.

While the systematic concerns of the first search are closely related to those of the FSD, the latter search requires that the correct $t = 0$ be established for every tile of the detector. Using coincident timing information from the calorimeter, the time offsets for every PSD stick can be determined, on a run-by-run basis, and the hits in the tiles aligned with the calorimeter within a 25 ns time window. Moreover, since the phase is a strong function of the decay positron energy, an elaborate program of gain balancing was also required. First, the overall gain of each calorimeter was established, on a run-by-run basis. To this end, the very linear region of the energy distribution, from about 60% to 90% of the maximum, was fit to a straight line. The x intercept was taken as the energy end point, 3.1 GeV. To minimize pulse pileup, only data taken more than 250 μs after injection were included in the calibration energy spectra. After energy scale adjustments and corrections for timing offsets, calorimeter times and energies could be matched with a PSD vertical coordinate. A similar calibration procedure then established *position dependent* energy end points. In this case, where because of shower leakage energy end points are not expected to sit at 3.1 GeV, the spectra were matched to the predictions of a complete tracking and detector simulation.

Time-dependent detector response can be misinterpreted as an EDM signal. Variations in gain with time were studied separately and eliminated by applying a time-dependent gain factor, $f(t, Y)$ for each Y tile. The correction function took the form

$$f(t, Y) = (1 + A_1 e^{-t/A_2})(1 + A_3 e^{-(t-A_4)^2/A_5^2}), \qquad (30)$$

where parameters $A_1 - A_5$ depend on the PSD vertical coordinate Y. Pulse pileup was corrected, on an average basis, in the time spectra [18]. Finally, time dependence arising from the cyclotron and vertical betatron motions of the beam were minimized with a simple digital filter.

In order to study systematic errors related to the CBO, in 2001 the storage ring was run at several different field indices n. Also, approximately two-thirds of the data were collected when the average radial magnetic field was about 10 ppm of the main vertical B field, which produced an average vertical beam displacement of 0.6 mm. After the radial field was zeroed, the alignment of the beam with respect to the detectors was much improved. Data taken before and after the magnetic radial field correction were analyzed separately. Data were also divided into subsets determined by different run conditions.

A few cuts were made to the data sample of PSD hits and calorimeter pulses. For single PSD cluster events (no sign of pileup) the energy was restricted to fall between 1.4 and 3.4 GeV. Fits to time spectra were started no earlier than 32 μs after injection. Table IV lists the total number of events (after cuts and before pileup subtraction) for the PSD analyses.

A. Details of the two PSD Analyses

1. Phase method

The ratio method [18] was used to determine the $g - 2$ phase vs vertical coordinate for each of the 20 horizontally directed tiles on each detector. The three parameter (A, ω, and Φ) fits of the ratio method are particularly insensitive to any residual slow variations in detector performance. The phase vs vertical coordinate plot was then fit to the 4-parameter function

$$\Phi(y) = p_0 + p_1(y - p_2) + |p_3(y - p_2)|, \qquad (31)$$

where p_1, which is proportional to the EDM, describes the up–down asymmetry (see [25] for details including the determination of the proportionality constant used below). Parameter p_3 accounts for phase changes not related to the EDM signal, p_2 corresponds to the vertical detector offset, and p_0 is an overall detector phase offset. The result of the fit for one detector, for one data set, is plotted in Fig. 13 and the p_1 variable for all PSD fits, both before and after the radial magnetic field correction are plotted versus the PSD station in Fig. 14.

2. Vertical position vs time method

The vertical position vs time method is modeled closely on that used in the analysis of the FSD data and serves as a cross-check on the phase vs vertical position analysis. For each PSD station, the average vertical position and rms width were fit vs time. The rms vertical width was fit first in order to determine the CBO period and lifetime parameters (T_{CBO} and τ_{CBO}), which were then fixed in the fit of the mean vertical position. The rms vertical width distribution

TABLE IV. Number of decay electrons used for PSD data analysis (in millions).

Data set	PSD 1	PSD 2	PSD 3	PSD 4	PSD 5	PSD (5 stations)
Before B correction $n = 0.122$	66	56	61	42	70	295
Before B correction $n = 0.142$	61	54	60	44	71	290
After B correction $n = 0.122$	83	73	76	65	93	390
Total	185	157	173	139	209	975

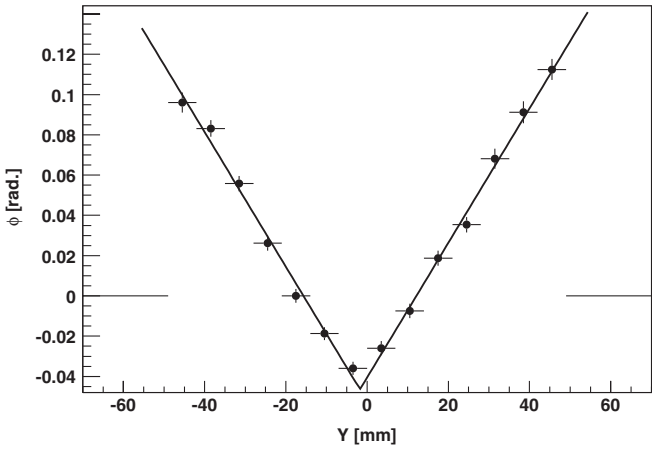

FIG. 13. PSD analysis: PSD 15 before B_r change. Phase of $g-2$ oscillation vs vertical position, with fit to Eq. (31). p_1, the EDM-sensitive parameter, describes any asymmetry between the two sides of the graph.

vs time was fit to the 9-parameter function:

$$f_{\rm rms}(t) = a_0 + A_1 \sin\left(\frac{2\pi t}{T}\right) + B_1 \cos\left(\frac{2\pi t}{T}\right) + A_2 \sin\left(\frac{4\pi t}{T}\right) + B_2 \cos\left(\frac{4\pi t}{T}\right) + e^{-(t/\tau_{\rm CBO})}\left(A_{\rm CBO} \sin\left(\frac{2\pi t}{T_{\rm CBO}}\right) + B_{\rm CBO} \cos\left(\frac{2\pi t}{T_{\rm CBO}}\right)\right), \quad (32)$$

where a_0 is the average PSD profile width. The time bin width was set to the cyclotron period, 149.185 ns, in order to average out oscillations in the time distribution caused by the bunched structure of the beam in the storage ring.

The parameters $T_{\rm CBO}$, $\tau_{\rm CBO}$, and T, the muon spin precession period $(2\pi/\omega)$ are all fixed. In particular, T is set to the nominal value 4365.4 ns. The rms width oscillations contain precession frequency terms A_1 and B_1, double precession frequency terms A_2 and B_2 due to the changes in average energy, detector acceptance, and time of flight of the decay electron within the precession period. CBO frequency terms $A_{\rm CBO}$ and $B_{\rm CBO}$ arise because of a variation in the decay electron time of flight with radius.

Next, the vertical mean position versus time is fit to a similar function:

$$f_{\rm Ave}(t) = y_0 + A_{g2} \sin\left(\frac{2\pi t}{T}\right) + B_{g2} \cos\left(\frac{2\pi t}{T}\right) + A_{2g2} \sin\left(\frac{4\pi t}{T}\right) + B_{2g2} \cos\left(\frac{4\pi t}{T}\right) + e^{-t/\tau_{\rm CBO}} \times \left[S_{\rm CBO} \sin\left(\frac{2\pi t}{T_{\rm CBO}} + \Phi_{\rm CBO}\right) + C_{\rm CBO} \cos\left(\frac{2\pi t}{T_{\rm CBO}} + \Phi_{\rm CBO}\right)\right], \quad (33)$$

where y_0 describes any misalignment between the beam and the vertical center of the PSD. There are precession frequency sine and cosine terms, A_{g2} and B_{g2}, and double precession frequency terms A_{2g2} and B_{2g2} all with the $g-2$ period fixed. The absolute phase of each detector was chosen so that the $g-2$ number oscillation is described by B_{g2} and any EDM signal would appear in A_{g2}. There are also CBO sine and cosine terms, $A_{\rm CBO}$ and $B_{\rm CBO}$. The CBO decay time, period, and phase are fixed by the rms width fit.

As in the FSD analysis, the very large false EDM signal caused by detector misalignment [26] must be corrected. The EDM-sensitive parameter, A_{g2}, was plotted versus the PSD measured vertical detector offset y_0. The value of A_{g2} at $y_0 = 0$, obtained from a fit to a straight line, corre-

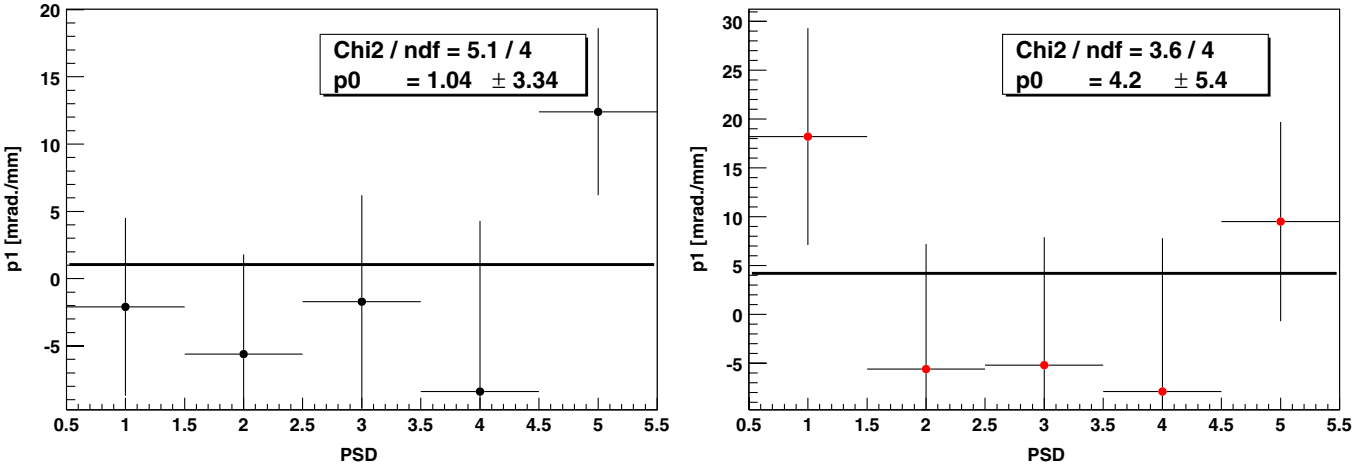

(a) Before B_r Correction (b) After B_r Correction

FIG. 14 (color online). PSD analysis: EDM-sensitive parameter p_1 [see Eq. (31)] versus PSD station. Horizontal lines indicate fits to a constant. p_1 is consistent with zero for both the data taken before and after B_R was changed (see text for discussion).

sponds, once again, to the EDM-related amplitude that would be measured by a perfectly aligned detector. Figure 15 shows the A_{g2} amplitude for the 5 PSD detectors, with separate points plotted for the data sets taken before and after the radial field correction.

B. Systematic errors

Systematic errors must be assessed separately for the two PSD analyses but most are similar to those of the FSD analysis. One of the largest systematic errors for the phase method is associated with the vertical alignment of the PSD with respect to the stored beam. To estimate the error, the relationship between the size of the false EDM signal and 1 mm of detector misalignment was established, using Monte Carlo simulation. The accuracy of the mean vertical position measurement was studied by imposing on the data a 10% tile inefficiency and 5% gain variation for top/bottom halves of the calorimeter. The estimated error in the vertical position is 0.2 mm. The Monte Carlo simulation was then used to determine the size of the false EDM signal produced per unit misalignment (see [25]), 140 μrad/mm. Multiplying that scaling factor by the estimated vertical misalignment yields an error of 29 μrad on p_1. The resulting error on the EDM is 0.74×10^{-19} e cm.

Since the intercept of the sine wave amplitude versus detector offset plot was used for the vertical position EDM measurement, detector misalignment was less important to the overall systematic error. In that case, the systematic uncertainty was estimated using the slope of the sine wave A_{g2} versus detector offset Y_o plot combined with the error in the detector offset measurement. The systematic error for the detector misalignment is 1.7 μm in A_{g2}, resulting in an EDM error of 0.2×10^{-19} $e$cm, as in Eqs. (26) and (27).

If the PSD is tilted with respect to the horizontal plane of the storage ring, horizontal beam oscillations produce apparent vertical oscillations in the average position measured by the PSD. The PSD tilt was estimated from a two-dimensional plot of PSD Y vs X coordinates, for data taken more than 32 μs after injection. The mean vertical position was calculated for each X tile and the ensemble of means was fitted vs X to a linear function. The tilt of five PSDs was consistent with 0 and no larger than 0.75 mrad on average.

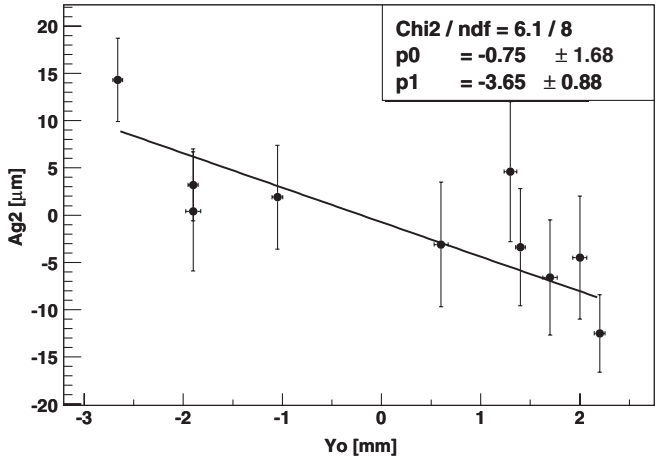

FIG. 15. PSD analysis: Fitted sine wave amplitude A_{g2} for the mean vertical position fit versus measured detector offset. A straight-line fit is overlaid. Since the intercept is consistent with 0, A_{g2} is directly proportional to the measured detector offset.

PSD tilt could also lead to asymmetric vertical losses which would affect the phase analysis. Higher energy electrons strike the calorimeter at larger radius, that is, closer to the storage region. Asymmetric losses could change the energy spectra and hence the phase of the detected electrons vs vertical coordinate. The size of the error was estimated with the full Monte Carlo simulation. The induced EDM signal in parameter p_1 per mrad of detector tilt is 26 μrad/mm (see [25]). Multiplying that scaling factor by the maximum tilt (0.75 mrad) yields an error 20 μrad/mm on p_1. The associated error on the EDM is 0.5×10^{-19} e cm.

As noted before, a time-dependent energy scale difference between the top and the bottom of the calorimeter can induce a false EDM signal. The energy balance procedure was checked by examining events in which the signal was restricted to the top or bottom of the calorimeter. The measured average top/bottom energy scale difference is less than 0.1% after the time-dependent energy correction was applied. Monte Carlo simulation indicates that a 1% top/bottom gain imbalance produces a 43 μrad/mm error, corresponding to an error of 4.3 μrad/mm in our case.

In order to study the error due to tile inefficiency, an artificial 10% inefficiency for tile 3 (for all PSDs) was imposed on the data. (Tile 3 corresponds to the uppermost tile used in the analysis.) The intercept change in Fig. 15 is only 1.8 μm, which is taken as an estimate of the systematic error for the vertical mean method.

Errors for the phase method are summarized in Table V. The total uncertainty is 50 μrad/mm on p_1, and 1.3×10^{-19} e cm on the EDM. Systematic uncertainties for the mean vertical position vs time method are presented in Table VI. The total systematic uncertainty for the vertical position method is 9.6 μm (or 1.1×10^{-19} e cm) and statistical error is 1.7 μm (or 0.2×10^{-19} e cm).

C. PSD Summary

Results from the two PSD analysis methods are consistent with zero and with each other. Averaged over the five PSD stations, the EDM signal from the phase analysis is $d_{\mu^-} = (-0.5 \pm 1.3) \times 10^{-19}$ e cm, where 0.7×10^{-19} e cm is the statistical error and 1.1×10^{-19} e cm is the systematic error. Averaged over the five PSDs, fitting the PSD vertical position versus time yields an EDM value of $d_{\mu^-} = (-0.1 \pm 0.7) \times 10^{-19}$ e cm, where 0.3×10^{-19} e cm and 0.7×10^{-19} e cm are the statistical and systematic errors, respectively.

TABLE V. Errors for the phase method. The first six entries of the center column list the size of a physical error and the sensitivity (assumed to be linear) of the EDM result to that error. The column to the right gives errors on EDM-sensitive parameter p_1 and in the totals, the error on the EDM itself.

Source	Sensitivity	Result
Detector Tilt	26 μrad/mm/mrad $\times$ 0.75 mrad	20 μrad/mm
Detector misalignment	138 μrad/mm/ mm $\times$ 0.2 mm	28 μrad/mm
Energy calibration	43 μrad/mm/% $\times$ 0.1%	4.3 μrad/mm
Muon vertical spin	1.0 μrad/mm $\times$ 8%	8.0 μrad/mm
Radial B field	0.72 μrad/mm/ppm $\times$ 20.0 ppm	14.4 μrad/mm
Timing	17.0 μrad/mm/ns $\times$ 0.2 ns	3.4 μrad/mm
Total systematic		38 μrad/mm (0.93×10^{-19} e cm)
Total statistical		28 μrad/mm (0.73×10^{-19} e cm)
Total		47 μrad/mm (1.2×10^{-19} e cm)

TABLE VI. Errors for the mean position method. The first five entries of the center column list the size of a physical error and the sensitivity (assumed to be linear) on the residual value of the EDM-sensitive parameter A_{g2} for a nomiminal detector offset of 0. In the last three rows, the systematic, statistical, and total errors on the EDM are also given.

Source	Sensitivity	Result
Detector misal.	4.1 μm/mm $\times$ 0.4 mm	1.6 μm
Detector tilt	3.0 μm/mrad $\times$ 0.75 mrad	2.3 μm
Energy calibration	28.0 μm/% $\times$ 0.1%	2.8 μm
Muon vertical spin	0.4 μm/% $\times$ 8%	3.2 μm
Radial B field	0.13 μm/ppm $\times$ 20 ppm	2.6 μm
Timing		1.5 μm
Tile ineff.		1.7 μm
Fitting		1.0 μm
Total systematic		6.2 μm (0.7×10^{-19} e cm)
Total statistical		1.7 μm (0.2×10^{-19} e cm)
Total		6.4 μm (0.7×10^{-19} e cm)

VIII. COMBINATION OF EDM RESULTS

The traceback data set is entirely independent of those used for the FSD and PSD analyses and there are minimal correlations between the systematic errors of the traceback analysis and those of the other two.

The combined measurement from the traceback and FSD analyses on the μ^+ is $d_{\mu^+} = (-0.1 \pm 1.0) \times 10^{-19}$ e cm, providing a limit on the permanent electric dipole moment of the positive muon of

$$|d_{\mu^+}| \leq 2.1 \times 10^{-19}\ e\,\text{cm (95\% C.L.)}. \qquad (34)$$

The μ^- result is taken from the PSD mean vertical position analysis: $d_{\mu^-} = (-0.1 \pm 0.7) \times 10^{-19}$ e cm with corresponding limit

$$|d_{\mu^-}| \leq 1.5 \times 10^{-19}\ e\,\text{cm (95\% C.L.)}. \qquad (35)$$

It is important to note that the errors on the traceback measurement are entirely statistical while those of the FSD and PSD measurements are dominantly systematic. Although the increased vertical segmentation of the BNL detectors is a distinct improvement over the two-paddle CERN III approach, significant further progress with this basic technique would be exceedingly difficult. In contrast, relatively simple remedies—increasing the geometric acceptance and reducing or eliminating the recovery period after injection—would lead to direct improvements in the traceback result.

In determining joint results from the μ^+ and μ^- data sets, we must consider the correlation of errors in the FSD(μ^+) and PSD(μ^-) analyses. While the FSD and PSD data sets are entirely independent, three of the systematic errors, the vertical spin, top/bottom calibration, and radial B-field errors, are correlated and, although it is impossible to judge the extent of the correlation, one might assume that the B and E fields of all bending and focusing elements are exactly reversed when changing from positive to negative beam and that these three errors are fully correlated.

The EDMs of the μ^+ and μ^- are found to be in accord with the *CPT* requirement that $d_{\mu^+} = -d_{\mu^-}$, or, in terms of directly measured quantities, $\eta_{\mu^+} = \eta_{\mu^-}$. The result is

TABLE VII. Summary of EDM results from the CERN III experiment and from the three analyses of E821. The units are $\times 10^{-19}\ e \cdot \mathrm{cm}$ in all cases. In combining the positive and negative muon results for the CERN experiment, we choose to cite the EDM for the negative muon.

Analysis	Mean value	Stat. error	Syst. error	Total error	95% C.L.
CERN (1978)					
(μ^+)	8.6	4.0	2.0	4.5	
(μ^-)	0.8	3.8	2.0	4.3	
Combined $\mu^+\mu^-$	−3.7	2.8	2.0	3.4	10.5
E821					
Traceback (μ^+)	0.0	1.6	0.1	1.6	
FSD (μ^+)	−0.1	0.7	1.2	1.4	
Average μ^+	−0.1	0.6	0.8	1.0	
PSD (μ^-)	−0.1	0.3	0.7	0.7	
Combined $\mu^+\mu^-$	0.0	0.2	0.9	0.9	1.8

$$d_{\mu^-} + d_{\mu^+} = (-0.2 \pm 1.3) \times 10^{-19}\ e\,\mathrm{cm}, \tag{36}$$

consistent with zero. In summing the results for μ^+ and μ^- to construct this difference, the correlated systematic errors in the FSD and PSD analyses should tend to cancel, as described above. However, because of uncertainties in the extent of the correlation, as a conservative measure, we take them to be completely uncorrelated.

Under the assumption of CPT invariance, we take a weighted average of the μ^- result and the opposite of the μ^+ results. In this case, once again as a conservative measure, we take the three correlated errors of the FSD and PSD analyses to contribute maximally to the total error. All other errors are added in quadrature. We obtain

$$d_\mu = (0.0 \pm 0.9) \times 10^{-19}\ e\,\mathrm{cm}. \tag{37}$$

This corresponds to the limit

$$|d_\mu| \leq 1.8 \times 10^{-19}\ e\,\mathrm{cm}\ (95\%\ \mathrm{C.L.}), \tag{38}$$

approximately a factor of 5 improvement over the previous limit. A summary of the results from each detector system, as well as those from CERN III, is shown in Table VII.

The observed difference between the standard model and the experimentally determined values of the muon anomaly, $\delta a_\mu = 295(88) \times 10^{-11}$ [27], could be attributed, in principle, to a shift in the muon spin precession frequency caused by a nonzero EDM; see Eq. (16). This would lead to an EDM of $d_{\delta a_\mu} = \pm 2.39(0.36) \times 10^{-19}\ e\,\mathrm{cm}$. The probability that $d_{\delta a_\mu}$ is compatible with the limit from Eq. (37) is 2%, suggesting it is unlikely that δa_μ arises from a nonzero EDM.

ACKNOWLEDGMENTS

We thank the BNL management, along with the staff of the BNL AGS for the strong support they have given the muon $(g-2)$ experiment over a many-year period. This work was supported in part by the U.S. Department of Energy, the U.S. National Science Foundation, the German Bundesminister für Bildung und Forschung, the Alexander von Humboldt Foundation, the Russian Ministry of Science, and the U.S.-Japan Agreement in High Energy Physics.

[1] A. D. Sakharov, JETP Lett. **5**, 24 (1967).
[2] F. Farley *et al.*, Phys. Rev. Lett. **93**, 052001 (2004).
[3] W. C. Griffith *et al.*, Phys. Rev. Lett. **102**, 101601 (2009).
[4] B. C. Regan *et al.*, Phys. Rev. Lett. **88**, 071805 (2002).
[5] C. A. Baker *et al.*, Phys. Rev. Lett. **97**, 131801 (2006).
[6] J. Bailey *et al.*, J. Phys. G **4**, 345 (1978).
[7] I. B. Khriplovich and R. A. Korkin, Nucl. Phys. **A665**, 365 (2000).
[8] O. Lebedev *et al.*, Phys. Rev. D **70**, 016003 (2004).
[9] M. Pospelov and A. Ritz, Ann. Phys. (N.Y.) **318**, 119 (2005).
[10] C. P. Liu and R. G. E. Timmermans, Phys. Rev. C **70**, 055501 (2004).
[11] C. A. Baker *et al.*, Phys. Rev. Lett. **97**, 131801 (2006).
[12] K. S. Babu *et al.*, Phys. Rev. Lett. **85**, 5064 (2000).
[13] R. M. Carey *et al.* (Muon $(g-2)$ Collaboration), Phys. Rev. Lett. **82**, 1632 (1999).
[14] H. N. Brown *et al.* (Muon $(g-2)$ Collaboration), Phys. Rev. D **62**, 091101 (2000).
[15] H. N. Brown *et al.* (Muon $(g-2)$ Collaboration), Phys. Rev. Lett. **86**, 2227 (2001).
[16] G. W. Bennett *et al.* (Muon $(g-2)$ Collaboration), Phys. Rev. Lett. **89**, 101804 (2002).
[17] G. W. Bennett *et al.* (Muon $(g-2)$ Collaboration), Phys.

Rev. Lett. **92**, 161802 (2004).
[18] G. W. Bennett *et al.* (Muon ($g - 2$) Collaboration), Phys. Rev. D **73**, 072003 (2006).
[19] J. Bailey *et al.*, Phys. Lett. B **55**, 420 (1975).
[20] J. Bailey *et al.*, Nucl. Phys. **B150**, 1 (1979).
[21] G. T. Danby *et al.*, Nucl. Instrum. Methods Phys. Res., Sect. A **457**, 151 (2001).
[22] S. A. Sedykh *et al.*, Nucl. Instrum. Methods Phys. Res., Sect. A **455**, 346 (2000).
[23] P. Cushman *et al.*, Nucl. Instrum. Methods Phys. Res., Sect. A **378**, 116 (1996).
[24] M. J. Sossong, Ph.D. thesis, University of Illinois (Urbana) [UMI-31-13195, 2005].
[25] S. Giron, Ph.D. thesis, University of Minnesota [UMI-29261, 2004], http://www.hep.umn.edu/theses.
[26] R. McNabb, Ph.D. thesis University of Minnesota [UMI-31-13195, 2003], http://www.hep.umn.edu/theses.
[27] J. P. Miller, E. de Rafael, and B. L. Roberts, Rep. Prog. Phys. **70**, 795 (2007).